Quasielastic neutron scattering reveals the temperature dependent rotational dynamics of densely grafted oleic acid.

[1]Aakash Sharma*, [1]Margarita Kruteva*, [2]Michaela Zamponi,[1]Sascha Ehlert, [1]Dieter Richter and [1]Stephan Förster

Affiliations

[1]Forschungszentrum Jülich GmbH, Jülich Centre for Neutron Science (JCNS-1: Neutron Scattering and Biological Matter), 52425 Jülich, Germany

[2]Forschungszentrum Jülich GmbH, Jülich Centre for Neutron Science at MLZ, Lichtenbergstraße 1, 85748 Garching, Germany

Author to whom correspondence should be addressed:
*Aakash Sharma: a.sharma@fz-juelich.de
*Margarita Kruteva: m.kruteva@fz-juelich.de

Abstract

We study the dynamics of pure oleic acid as well as grafted oleic acid synthesized by decomposing iron oleate into oleic acid grafted iron oxide nanoparticles. Our quasielastic neutron scattering study shows that oleic acid dominantly performs translational diffusion at room temperature. On the other hand, in nanocomposites the constraints imposed by grafting and crowding of neighbouring chains restrict the grafted oleic acid to uniaxial rotation. Interestingly, it also manifests mobility in grafted oleic acid below the crystallization temperature of pure oleic acid. The data from grafted oleic acid could be effectively described using uniaxial rotational diffusion model with an additional elastic scattering contribution. This kind of elastic scattering arises due to the restricted bond mobility and increases with decreasing temperature. The radius of rotation obtained from the fitted data agrees very well with the geometry of the molecule and grafting density. These results open possibilities of research on the confined surfactant systems, which could be analysed using the approach described here.

I. Introduction

Fatty acids and surfactants form essential part of our life. Oleic acid is a well know fatty acid which is naturally found in edible oils e.g. olive and peanut oil. The medicinal effects of oleic acid on the immune system are studied by many researchers.[1,2] The applications of oleic acid have also been explored in the treatment of cancer and other diseases.[1–4] Other than medical field and pharmaceuticals, oleic acid is also well utilized in the field of material science as a surfactant.[5,6] One of the major uses of oleic acid is in the area of nanocomposites. Oleic acid is used to stabilize nanocomposites by altering the surface interaction between nanoparticles and the matrix.[7,8] For example, silica nanoparticles are coated with oleic acid to enhance the dispersity of silica in polymers like polystyrene.[9] Metal oleates are decomposed at high temperatures to form nanocrystals that are grafted with oleic acid.[8] These nanoparticles are useful for many application e.g. in sensors, polymer nanocomposites catalysis etc.[6] Iron oxide nanocrystals stabilized by oleic acid exhibit enhanced magnetic performance as compared to the ungrafted iron oxide particles.[10] The structure and properties of these oleic acid stabilized nanoparticles have been studied in detail.[11,12]

Structure and phase behaviour of oleic acid has been studied using experiments as well as simulations.[4,13–16] Self-assembly of oleic acid and water into different phases was investigated by MD simulations.[4] Tandon et al.[17] have used X rays and Raman spectroscopy to follow the phase transition between different crystalline forms of pure oleic acid. When crystallized from melt state, oleic acid crystallizes in two different forms α and γ subsequently at temperatures below room temperature. In the γ form, the oleic acid molecules exit in skew–cis–skew' conformation and transitions to a skew–cis–trans conformation in the α form. A strong influence of temperature on the conformation change of oleic acid has been shown.[18] Increasing temperature of the γ crystalline form leads to faster dynamics of the methyl group which gives a pathway to disordering of oleic acid and formation of α phase. Thus, there is plenty of literature present on the effect of temperature on the conformational change of oleic acid. On the other hand, the dynamics of oleic acid has been studied by fewer researchers.[3,5] Especially, dynamics of oleic acid or other surfactants in a confined environment have not been well studied.

Dynamics of polymer chains grafted on nanoparticles have been investigated by many researchers as well as our group.[19–22] It has been found that on grafting the polymer chains on nanoparticles, their dynamics is retarded. Whereas, there are limited results on the dynamics of short molecules like oleic acid in spatially confined environments.[23–26] Literature reports show that the quasielastic scattering from a

monolayer of short chains on nanocrystal surfaces could be described by a combination of precession as well as rotation about a central axis. Seydel et. al.[26] analysed the Time of Flight data from oleic acid monolayer on PbS nanocrystals. However, the experiments were performed on particles dispersed in a solvent. There are few reports on the dynamics of oligomers grafted on nanoparticles using techniques like molecular dynamics simulations and dielectric spectroscopy.[27,28] Holt et al.[27] showed using dielectric spectroscopy that the segmental dynamics of oligomers slows down on grafting but secondary motions like β relaxation become faster as compared to pure oligomers. Molecular dynamics simulations by Hong et al.[28] showed the dynamics of poly(ethylene oxide) oligomers becomes faster than the bulk oligomer at lower temperatures whereas, retards at high temperatures. Dynamics of short chain alkanes and liquid crystals have also been studied in literature using quasielastic neutron scattering.[29–31] Despite of the fact that oleic acid grafted nanoparticles are commonly used in various application,[2,11] there is limited data reported on the dynamics of free and grafted oleic acid molecules.

Here we investigate the dynamics of oleic acid in ungrafted as well as grafted state without any solvent using simplistic, yet physical, analytical approaches. We show that quasielastic neutron backscattering can be effectively used to investigate the critical features of the dynamics of oleic acid. Neutron backscattering is a space as well as time resolved spectroscopy tool that is utilized to explore dynamics at the length scales on the order of a nanometre.[32] We present sophisticated methodologies for analysing the quasielastic neutron scattering data from ungrafted and grafted oleic acid. Our results show that due to grafting, the oleic acid exhibits dynamics even at temperatures lower than crystallization temperature of pure oleic acid. The analysis presented here captures the effect of temperature on the physical parameters that govern oleic acid mobility in grafted form. The results have been quantitatively correlated to the geometrical restrictions imposed on the oleic acid by the grafting sites and molecule's dimensions. The methodology utilized by us is generic and could be used to analyse the dynamics in similar systems of short surfactant like molecules grafted to a surface or in free form.

II. Experiment

A. Material

Iron chloride $FeCl_3.6H_2O$ (99%), octadecene (for synthesis), heptane (99%), oleic acid (technical grade), and acetone (pro analysis) were purchased from Sigma-Aldrich and used as received. Ethanol (99%) was purchased from VWR and used as received. Sodium oleate (97%) was purchased from TCI and used as received. The synthesis of iron oleate and iron oxide nanoparticles were carried out using a published procedure.[8] In short, sodium oleate was reacted with iron chloride to generate iron oleate complex. Iron oleate complex was decomposed by heating at 320°C in octadecene. This gave rise to iron oxide nanoparticles with oleic acid grafted on their surface. The grafting density of oleic acid as measured by thermogravimetric analysis (TGA) is 3 chains/nm^2.

B. Neutron Backscattering

Neutron backscattering captures dynamics at short length scales on the order of a nanometre. Backscattering experiments were performed on SPHERES operated by JCNS at MLZ, Garching.[33] The energy resolution is about 0.65 μeV, an energy range ($\hbar\omega$) of -30 to 30 μeV was used at a wavelength (λ) of 6.271 Å. Data was obtained in a Q range of 0.6 – 1.7 Å^{-1}. We measured vanadium as reference and used the vanadium spectra to normalized our backscattering data in order to correct for detector efficiencies and geometrical effects. Scattering from an empty cell was subtracted as background. We measured backscattering spectra for each sample at four different temperatures: 3 K, 250 K, 275 K and 300 K. The data at 3 K was used to determine the instrument resolution. This resolution was convoluted with our model functions during fitting. We used Jscatter software[34] to fit the corrected data sets at 250 K, 275 K and 300 K. Next section describes the fitting functions that we used to model the backscattering spectra.

C. Fitting functions:

Kohlrausch–Williams–Watts (KWW)

We use the phenomenological KWW function to fit neutron backscattering intensities, related to the dynamic structure factor, S(Q, ω). The KWW function is a stretched exponential function, which is defined in the time domain. In order to fit the neutron backscattering data in frequency domain, we numerically converted the time domain KWW function employing a Fourier transformation:

$$S(Q,\omega) = \mathcal{F}\left[\mathrm{Amp} \times \exp\left[-\left(\frac{t}{\tau(Q)}\right)^{\beta}\right]\right] \quad (1)$$

where, ω is the frequency, Amp is the amplitude, t is the time, τ(Q) is the KWW relaxation time that depends on the scattering vector (Q), and β is the stretching parameter. $\mathcal{F}$ represents the Fourier transformation of KWW function into frequency domain.

The KWW function is useful to capture complicated relaxation processes that could not be fitted using a single exponential function. The stretching of exponential function may represent heterogenous relaxation but could also indicate intrinsic sub-diffusive motion. In the first case a

lower value of β indicates increasingly heterogenous relaxation. τ (Q) is a characteristic relaxation time of the KWW function however, it is not the average relaxation time. Based on the values of τ and β, the average relaxation time (τ_o) is calculated as:

$$\tau_o = \frac{\tau}{\beta}\,\Gamma\left[\frac{1}{\beta}\right] \tag{2}$$

where Γ is gamma function.

For centre of mass diffusion, the dynamic structure factor decays are e^{-Q^2Dt} and thus the relaxation time and diffusion coefficient are related as:

$$D \sim \frac{1}{Q^2\tau_o} \tag{3}$$

Uniaxial rotation model:

The uniaxial rotation model describes the rotation of a molecule around its principal axis. Therefore, it is suitable to model the rotational motion of short chain molecules that are confined in such a way that their translational movement is restricted by neighbouring constraints. Such chains relax dominantly by rotation around their principal axis. The dynamic scattering factor from this model has been derived by Dianoux et al.[30] and M. Bée.[35] In order to describe the data from grafted oleic acid, we invoke the uniaxial rotation model. The amplitude Amp comprises the Debye Waller factor and possible normalization errors. Here we present the final theoretical result for the uniaxial rotation model - the detailed derivation could be found in reference.[30] The incoherent scattering function $S_{rot}(Q, \omega)$ is derived as:

$$S_{rot}(Q,\omega) = \mathrm{Amp}\left[J_0^2(Q\,r\sin\theta)\delta(\omega) + \frac{2}{\pi}\sum_{n=1}^{\infty} J_n^2(Q\,r\sin\theta)\,\frac{D_r n^2}{(D_r n^2)^2+\omega^2}\right] + \mathrm{bgr} \tag{4}$$

where, r is the radius of rotation, θ is the angle between rotational axis and scattering vector Q. J_n is the Bessel function of n^{th} order, D_r is the rotational diffusivity and bgr is a background contribution that e.g. may arise from fast relaxational motions.

In order to fit the data, we orientationally averaged equation 4 with respect to the angle between scattering vector (Q) and axis of rotation over 4π. We vary the value of n in different fits to estimate the convergence of equation 4 in case of our data. We conclude that the terms beyond n=5 are inconsequential to the fit quality and fitting parameters. However, in order to ensure stability and uniqueness of the solution, we fixed the maximum value of n at 10.

III. Results and discussions

A. Oleic Acid

Figure 1(a) shows a representative backscattering spectrum for oleic acid measured at 300 K and Q = 1.12 Å^{-1}. Here we also plot the indicative instrument resolution as dashed line at the same Q value. We notice a broad backscattering spectrum for oleic acid, which indicates the presence of fast motional processes. This is anticipated for a small molecule like oleic acid. The data is fitted using the KWW function of equation 1. We observe that the stretching exponent β varies in the range of 0.48 – 0.65. The average relaxation times (τ_o) are obtained for each Q value using equation 2 as shown in Figure 1(b). We observe that τ_o decreases with Q as $\tau \propto Q^{-2}$ as indicated by dashed black line.

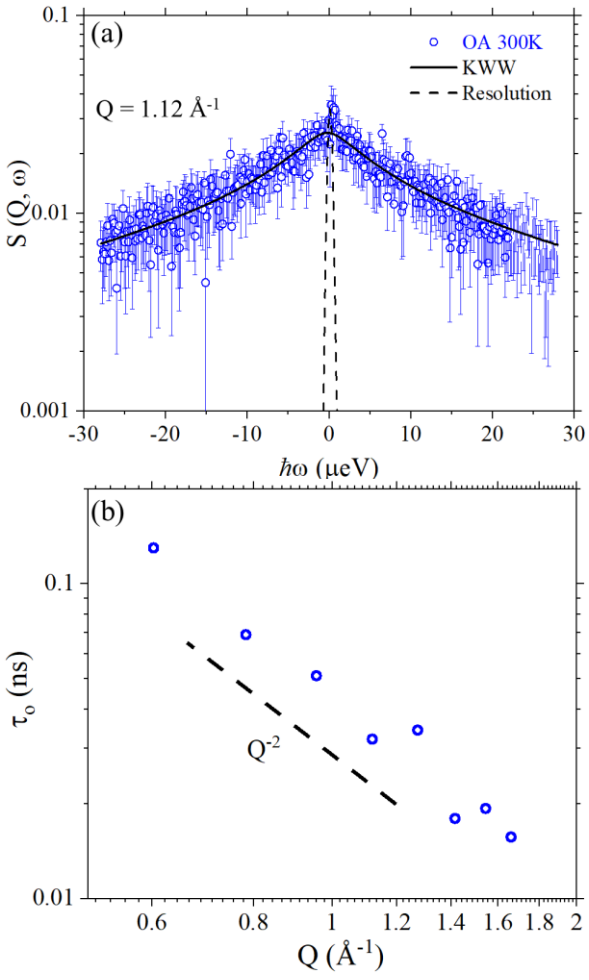

Figure 1. (a) Representative backscattering spectrum from pure oleic acid measured at Q = 1.12 Å^{-1} at 300 K. Black

line represents KWW fit to the data and dashed line indicates instrument resolution (b) variation of average relaxation times with Q values for oleic acid at 300 K.

The broadness of the backscattering spectrum in Figure 1(a) advocates high mobility of the oleic acid molecules. The variation of the average relaxation times as Q^{-2} indicates a relaxation process that is governed by diffusion. There are different kinds of relaxation processes that could contribute to the observed dynamics. For example, vibrational and librational motion, rotational and translational diffusion etc. Vibrational motions occur at very short time scales and therefore, we expect negligible contribution from these dynamics in the backscattering energy window. On the other hand, rotational and translational motions are the major contributors to the spectra in the time frame of backscattering. Interestingly, we obtain stretching parameter $\beta < 1$, which indicates that there are additional contributions to the quasielastic scattering from internal motions of oleic acid molecule. However, τ_0 follows a clear Q^{-2} power law therefore, we anticipate that the translational diffusion dominates the overall dynamical response of oleic acid molecule. Following equation 3, with this assumption, we calculate the respective average diffusion coefficients (D). Figure 2 displays the values of D at different Q values.

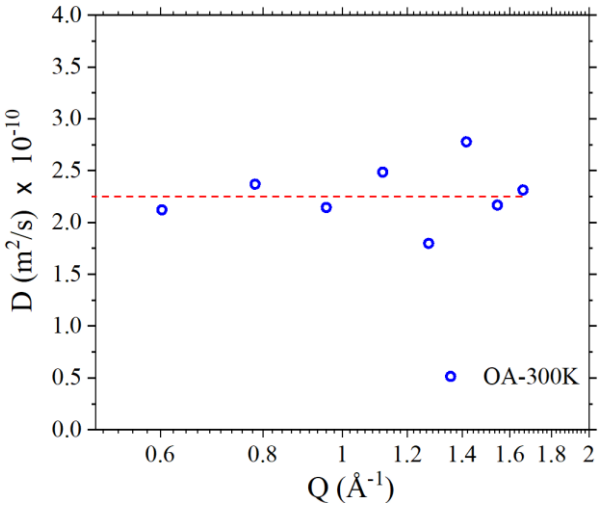

Figure 2. Oleic acid diffusivities calculated using equation 3 at different Q values at 300 K. Red line represents the average diffusivity.

From Figure 2 we notice that the diffusivities vary in a range of 1.9 – 2.4 x 10^{-10} m^2/s with an average value ~2.25 x 10^{-10} m^2/s. This result is in good agreement with literature values for similar fatty acids.[36] Thus, the simple approach of using KWW functions results in reasonable values for diffusion and relaxation times for pure oleic acid within the error values.

Oleic acid is known to crystallize at ~286 K.[37] We performed backscattering experiments on pure oleic acid at 275 K and 250 K. At these temperatures the backscattering data consist of only elastic scattering as shown in the Figure S1 of supporting information. Therefore, below the crystallization temperature, we do not observe signatures of any relaxation process. This is in line with the anticipation of a crystalline structure. Next, we study oleic acid nanocomposites where the oleic acid is grafted on iron oxide nanoparticles.

B. Oleic acid nanocomposite

The Oleic acid nanocomposite consists of oleic acid grafted on the surface of iron oxide nanoparticles. In order to follow the crystallisation phase transition in pure oleic acid and oleic acid nanocomposite, we performed elastic fixed window scans using the neutron backscattering instrument SPHERES. While the sample is gradually heated up from 3 to 300 K at 0.66 K/min, the elastic intensity is measured continuously during the temperature change. Results for the elastic scattering within the resolution window of SPHRES during the temperature scan at Q = 1.12 $Å^{-1}$ are shown in Figure 3.

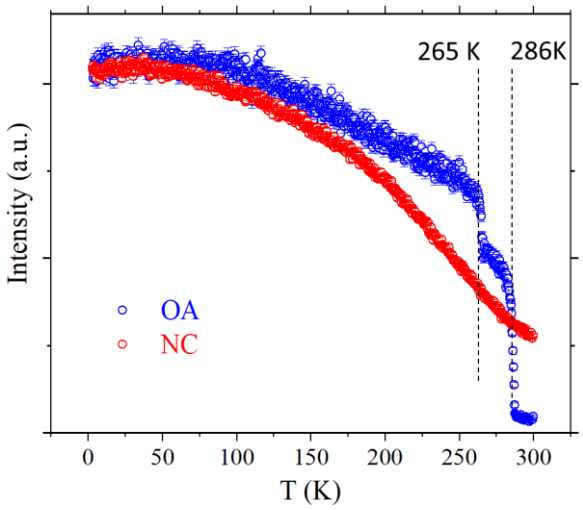

Figure 3. Temperature scan of the elastic neutron scattering intensity within the resolution window of SPHERES from oleic acid and the nanocomposite. Vertical dashed lines indicate the phase transition temperatures in oleic acid in α (286 K) and γ (265 K) crystalline states. Such transitions are absent in the nanocomposite.

As shown in Figure 3, we notice the clear signature of crystallization of pure oleic acid from melt state to the α phase at ~286 K and to the γ phase at ~267 K.[17] On the other hand, such phase transitions are absent in the data from the nanocomposite. We confirmed this result on the nanocomposite by Differential Scanning Calorimetry (DCS)

measurements as a complementary technique (Figure S2 of supporting information). We conclude that grafting precludes the possibility of crystallization of oleic acid even at such high grafting density of 3 chains/nm^2. Interestingly, the temperature scan data instructs that motion in grafted oleic acid even at temperatures below its crystallization temperature is taking place.

In order to quantify these motions, we performed backscattering experiments on the oleic acid nanocomposites at two temperatures below the crystallization temperature of oleic acid i.e. at 250 K, 275 K and one temperature above its crystallization temperature at 300 K. Figure 4 shows representative backscattering spectra from the oleic acid nanocomposites at (a) 250 K, (b) 275 K and (c) 300 K. We observe significant broadening of the spectra at higher energy transfers even at low temperatures. This confirms the prediction of relaxation processes below the crystallization temperature on the basis of the temperature scan.

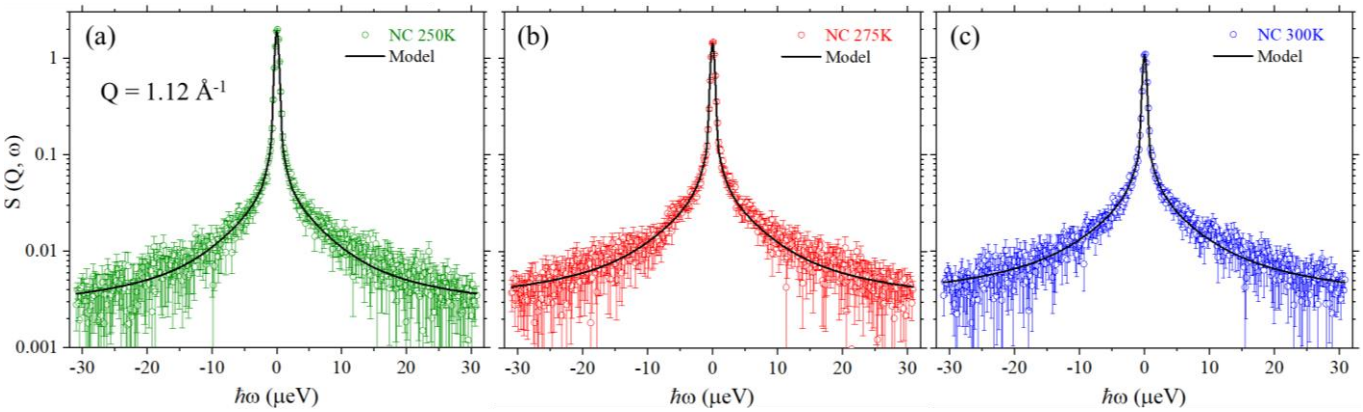

Figure 4. Representative backscattering spectra from grafted oleic acid nanocomposite at Q = 1.12 Å^{-1} at three different temperatures (a) 250 K (b) 275 K (c) 300 K. Black line represents the fit obtained using equation 5.

We also observe additional elastic scattering at all temperatures. These elastic contributions majorly originate from the spatial restriction in the oleic acid dynamics imposed by grafting, with negligible contribution from nanoparticles. As well, the presence of a broad backscattering signal at higher energy transfers indicates substantial dynamics. For simplicity, we initially analysed the data by fitting a KWW function similar to the pure oleic acid analysis. The KWW function is a phenomenological model and assumes nothing with respect to the governing physics of oleic acid dynamics. The representative fits are shown in Figure S3 of the supporting information. We observe that the fitted β values vary in an extraordinarily low range of 0.12 – 0.19. Such low β values would indicate a very wide distribution of relaxation times or diffusivities representing the presence of extremely slow as well as fast components imparted due to various dynamical contributions. Clearly, a simple KWW model does not prove to be much informative with regard to the dynamics in grafted oleic acid.

In order to select a better model for the analysis, we compare the size of oleic acid with the accessible distance between adjacent grafting sites. Figure 5 represents a schematic of the oleic acid grafted on a nanoparticle surface. The length of a stretched oleic acid molecule can be calculated using literature values[13] for the different bond lengths and bond angles as ~ 2.0 nm. This value is close to the measured value of the oleic acid length (~ 2.1 nm).[38] The width of oleic acid obtained from our calculations is ~ 0.5 nm. Due to grafting translational relaxation is out of the question, however, the molecule could undergo rotation around an axis. Further information is obtained by studying the grafting geometry. With a grafting density of about 3 the average distance between grafted molecules is $1/\sqrt{\sigma}$ = 0.58 nm, which compares well with the lateral molecular size of 0.5 nm. Thus, the oleic acid molecules are densely packed on the iron oxide surface. Comparison of surface area per molecule and the width of oleic acid encourage us to assume that the relaxation process in grafted oleic acid is dominated by uniaxial rotation of the molecule around its own chain axis. Therefore, we fitted the oleic acid nanocomposite data using uniaxial rotation model as presented in the equation 4.

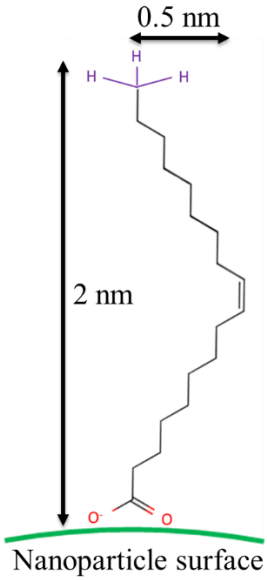

Figure 5. Schematic structure of the oleic acid molecule grafted on nanoparticle surface.

We observe that the fitted radius of rotation and rotational diffusivity (D_r) vary in a broad range across different Q values. Our attempts to fit the data using a common rotation radius and D_r were unsuccessful. Variation of D_r and r across Q values is unphysical. This indicates that the simple uniaxial rotation model is incapable of capturing the physics of the grafted oleic acid and a modification of this model is in order. We anticipate that grafting induces additional constraints on the mobility of oleic acid. Due to these constraints, the free rotation of some of the bonds might get restricted which gives rise to additional elastic scattering from the oleic acid molecule. Therefore, we introduce an additional constant elastic contribution (C) to the uniaxial rotation model as shown below:

$$S_{rot}(Q,\omega) = Amp\left[J_0^2(Q\,r\sin\theta)\delta(\omega) + C\,\delta(\omega) + \frac{2}{\pi}\sum_{n=1}^{\infty} J_n^2(Q\,r\sin\theta)\,\frac{D_r n^2}{(D_r n^2)^2+\omega^2}\right] + bgr \quad (5)$$

The fraction of additional elastic contribution is calculated as $\chi = \frac{C}{1+C}$. To further analyse the dynamics of the nanocomposites, we employ equation 5 to fit backscattering data. In order to obtain reliable quantities for each temperature, we perform joint fits for all Q values by keeping Dr, r and C as common fit parameters. This kind of global fit is justified as diffusivity, radius of rotation and additional elastic scattering is not expected to vary with Q values.

We observe that for initial fit results, the radius of rotation varied with temperature with higher radius of rotation for 300 K (r = 0.3 nm) and lower radius for lower temperatures i.e. r = 0.22 nm for 275 K and r = 0.19 nm for 250 K. However, the variation in radius of a molecule at lower temperatures goes against general intuition. Therefore, we fix the radius of rotation as r = 0.3 nm from 300 K to fit the data sets at 275 K and 250 K. This is based on the assumption that at higher temperatures, maximum number of bonds will be free to rotate hence, providing correct information of the effective molecular radius of rotation. The data along with the resulting fits (black lines) are shown in Figure 4 for one representative Q-value and all the temperatures. It may be seen from Figure 4 that the uniaxial rotation model with additional elastic scattering gives an excellent fit to the grafted oleic acid data, efficiently describing the elastic as well as the quasi-elastic part of the spectra. This also establishes that the failure of unmodified uniaxial rotation model to fit the data is not due to unaccounted fast relaxation processes but due to the confinement effects induced by grafting. The final fit results for the model parameters are given in Table 1.

Table 1. Fitted parameters for uniaxial rotation of grafted oleic acid.

	D_r (ns^{-1})	r (nm)	χ
250	2.06	0.3	0.52
275	2.34	0.3	0.39
300	2.7	0.3	0.28

We now discuss the physical significance of the resulting parameters. We compare the obtained values for radii of rotation with the geometry of oleic acid molecule and the accessible distance between the neighbouring anchor sites. The width of the oleic acid molecule as mentioned earlier is ~ 0.5 nm. The calculated distance between adjacent molecules at the grafting site (~ 0.58 nm) compares remarkably well with the fitted radius of rotation for grafted oleic acid (2 x 0.3 = 0.6 nm). This is an important result which supports the uniaxial rotation as the dominating relaxation process. It is noteworthy that our approach does not account for the rotation of individual hydrogen atoms. Therefore, the radius of rotation represents an effective radius of the cylindrical cross section spanned by grafted oleic acid molecule. Nonetheless, using this simple approach we are able to obtain physically justifiable rotational radius for grafted oleic acid.

At 300 K, the additional elastic contribution (χ = 0.28) is minimum as compared to 275 K (χ = 0.39) and 250 K (χ = 0.52). This indicates that at lower temperatures, the bond rotation is further restricted as compared to 300 K. An indication of this was observed by us in the initial fits where we obtained a temperatures dependent effective radius of rotation.

The values for the rotational diffusivities (D_r) decrease with lower temperatures. Decrease in diffusivity represents slow dynamics at lower temperatures, which is intuitive. We obtain corresponding activation energy from the variation of rotational diffusivity with temperature using an Arrhenius plot (supporting information Figure S4). The activation energy for grafted oleic acid is 3.3 kJ/mol. We observe that the rotational activation energy obtained for grafted oleic acid is in the same range of energies reported in the literature for other grafted ligand systems.[25]

We interpret that the oleic acid molecules rotate around their central axis similar to a cylindrically shaped molecule with some of the bond rotations restricted at 300 K. At lower temperatures even fewer bonds contribute to the observed rotational motion and other bonds cease to rotate in the backscattering window. This selective bond rotation at lower temperature gives rise to an increase in the overall elastic scattering leading to a higher value of χ. It should be noted that with this interpretation we do not claim that larger length scale bond rotations are frozen at 250 K. It is also possible that those motions are retarded to large extents such that their relaxation lies outside the energy window of backscattering spectroscopy. One can also not completely deny the possibility that temperature induced conformational changes at low temperatures[17] lead to a complete cessation of rotation of the bonds close to the grafting site. However, in order to validate these possibilities, one must perform further experiments, utilizing techniques that can probe lower frequency range for grafted oleic acid, which requires a separate study. Nevertheless, the uniaxial rotational diffusion model efficiently captures the effect of temperature on the structural dynamics of densely grafted oleic acid on a surface. Our results show that at sufficiently high grafting densities, uniaxial rotation is the dominant relaxation process whereas, for ungrafted oleic acid, translation diffusion dominates.

IV. Summary:

We have studied the dynamics of oleic acid in the melt as well as in the grafted state in form of grafted oleic acid nanocomposites using neutron backscattering. We observe vastly different features in the relaxation of ungrafted and the grafted oleic acid. We show that the pure oleic acid shows temperature dependent phase transition from melt to α and γ phase at lower temperatures. This leads to translational diffusion dominated relaxation at room temperature and crystallization induced elastic scattering at lower temperatures. On the other hand, the inability of grafted oleic acid to crystallize leads to a dynamic response even at lower temperatures. However, due to high grafting densities, the dynamics is considerably constrained by the neighbouring molecules. An efficient model to capture the dynamics assumes uniaxial rotation around the molecular axis. This approach helps to understand the effect of temperature on the mobility of grafted oleic acid in terms of decreased diffusivities and increased elastic scattering at lower temperatures. This framework utilizes a minimum number of fitting parameters yet, providing convincing explanation for the differences in the neutron scattering features from ungrafted and grafted oleic acid. We must emphasize that this framework can be utilized in general for confined surfactant and short chain systems.

SUPPLEMENTARY MATERIAL

See supplementary material for neutron backscattering spectra obtained from oleic acid at 250 K and 275 K, differential scanning calorimetry data from oleic acid nanocomposites, KWW fits of the oleic acid nanocomposites data, Arrhenius fit to the rotational diffusivities.

Acknowledgement

We acknowledge Amruta Sharma for differential scanning calorimetry measurements and Ralf Biehl for useful discussions.

AUTHOR DECLARATIONS

Conflict of Interest

The authors have no conflicts to disclose.

DATA AVAILABILITY

The data that support the findings of this study are available from the corresponding author upon reasonable request.

[1] M. del M. Cavia, C. Carrillo, and S. Alonso-Torre, Nutr. Hosp. **27**, 978 (2012).

[2] H. Sales-Campos, P. Reis de Souza, B. Crema Peghini, J. Santana da Silva, and C. Ribeiro Cardoso, Mini-Reviews Med. Chem. **13**, 201

(2013).

[3] R. Mohan, A. Jain, P. Tandon, S. Wartewig, and V. Dayal, Chem. Phys. Lipids **142**, 70 (2006).

[4] J.J. Janke, W.F.D. Bennett, and D.P. Tieleman, Langmuir **30**, 10661 (2014).

[5] C. Wei and A. Pohorille, J. Phys. Chem. B **118**, 12919 (2014).

[6] H. Heinz, C. Pramanik, O. Heinz, Y. Ding, R.K. Mishra, D. Marchon, R.J. Flatt, I. Estrela-Lopis, J. Llop, S. Moya, and R.F. Ziolo, Surf. Sci. Rep. **72**, 1 (2017).

[7] S. Ehlert, S.M. Taheri, D. Pirner, M. Drechsler, H.W. Schmidt, and S. Förster, ACS Nano **8**, 6114 (2014).

[8] J. Park, K. An, Y. Hwang, J.E.G. Park, H.J. Noh, J.Y. Kim, J.H. Park, N.M. Hwang, and T. Hyeon, Nat. Mater. **3**, 891 (2004).

[9] X. Ding, J. Zhao, Y. Liu, H. Zhang, and Z. Wang, Mater. Lett. **58**, 3126 (2004).

[10] S. Wang, F.J. Yue, D. Wu, F.M. Zhang, W. Zhong, and Y.W. Du, Appl. Phys. Lett. **94**, 2 (2009).

[11] M. Basini, T. Orlando, P. Arosio, M.F. Casula, D. Espa, S. Murgia, C. Sangregorio, C. Innocenti, and A. Lascialfari, J. Chem. Phys. **146**, (2017).

[12] P. De La Presa, M. Multigner, J. De La Venta, M.A. García, and M.L. Ruiz-González, J. Appl. Phys. **100**, (2006).

[13] F. Kaneko, K. Yamazaki, K. Kitagawa, T. Kikyo, M. Kobayashi, Y. Kitagawa, Y. Matsuura, K. Sato, and M. Suzuki, J. Phys. Chem. B **101**, 1803 (1997).

[14] Y. Kim, H.L. Strauss, and R.G. Snyder, J. Phys. Chem. **92**, 5080 (1988).

[15] M. Motoyama, Structure and Phase Characterization of Triacylglycerols by Raman Spectroscopy, 2012.

[16] C. Himawan, V.M. Starov, and A.G.F. Stapley, Adv. Colloid Interface Sci. **122**, 3 (2006).

[17] P. Tandon, G. Förster, R. Neubert, and S. Wartewig, J. Mol. Struct. **524**, 201 (2000).

[18] F. Pi, F. Kaneko, H. Shinzawa, M. Suzuki, M. Iwahashi, and Y. Ozaki, Bull. Chem. Soc. Jpn. **84**, 403 (2011).

[19] M. Jhalaria, E. Buenning, Y. Huang, M. Tyagi, R. Zorn, M. Zamponi, V. García-Sakai, J. Jestin, B.C. Benicewicz, and S.K. Kumar, Phys. Rev. Lett. **123**, (2019).

[20] C. Mark, O. Holderer, J. Allgaier, E. Hübner, W. Pyckhout-Hintzen, M. Zamponi, A. Radulescu, A. Feoktystov, M. Monkenbusch, N. Jalarvo, and D. Richter, Phys. Rev. Lett. **119**, 1 (2017).

[21] S.A. Kim, R. Mangal, and L.A. Archer, Macromolecules **48**, 6280 (2015).

[22] A. Sharma, M. Kruteva, M. Zamponi, S. Ehlert, D. Richter, and S. Förster, Phys. Rev. Mater. **6**, 1 (2022).

[23] R. Mukhopadhyay, S. Mitra, M. Johnson, V.R. Rajeev Kumar, and T. Pradeep, Phys. Rev. B - Condens. Matter Mater. Phys. **75**, 1 (2007).

[24] T. Pradeep, S. Mitra, A. Sreekumaran Nair, and R. Mukhopadhyay, J. Phys. Chem. B **108**, 7012 (2004).

[25] M. Jansen, F. Juranyi, O. Yarema, T. Seydel, and V. Wood, ACS Nano **15**, 20517 (2021).

[26] T. Seydel, M.M. Koza, O. Matsarskaia, A. André, S. Maiti, M. Weber, R. Schweins, S. Prévost, F. Schreiber, and M. Scheele, Chem. Sci. **11**, 8875 (2020).

[27] A.P. Holt and C.M. Roland, Soft Matter **14**, 8604 (2018).

[28] B. Hong and A.Z. Panagiotopoulos, J. Phys. Chem. B **116**, 2385 (2012).

[29] J.D. Barnes, J. Chem. Phys. **5193**, 5193 (1973).

[30] A.J. Dianoux, F. Volino, and H. Hervet, Mol. Phys. **30**, 1181 (1975).

[31] B. Ewen, G.R. Strobl, and D. Richter, Faraday Discuss. Chem. Soc. **69**, 19 (1980).

[32] E.J. Bailey and K.I. Winey, Prog. Polym. Sci. **105**, 101242 (2020).

[33] J. Wuttke, A. Budwig, M. Drochner, H. Kämmerling, F.J. Kayser, H. Kleines, V. Ossovyi, L.C. Pardo, M. Prager, D. Richter, G.J. Schneider, H. Schneider, and S. Staringer, Rev. Sci. Instrum. **83**, 1 (2012).

[34] R. Biehl, PLoS One **14**, e0218789 (2019).

[35] M. Bée, *Quasielastic Neutron Scattering* (1988).

[36] M. Iwahashi, Y. Kasahara, H. Matsuzawa, K. Yagi, K. Nomura, H. Terauchi, Y. Ozaki, and M. Suzuki, J. Phys. Chem. B **104**, 6186 (2000).

[37] M. Suzuki, T. Ogaki, and K. Sato, J. Am. Oil Chem. Soc. **63**, 553 (1986).

[38] E.R. Garland, E.P. Rosen, I. Clarke, and T. Baer, Phys. Chem. Chem. Phys. **10**, 3156 (2008).